NIST Author Manuscript

NIST Author Manuscript

NIST Author Manuscript

State Readout of a Trapped Ion Qubit Using a Trap-Integrated Superconducting Photon Detector

S. L. Todaro[1,2,†], **V. B. Verma**[3], **K. C. McCormick**[1,2,‡], **D. T. C. Allcock**[1,2,4], **R. P. Mirin**[3], **D. J. Wineland**[1,2,4], **S. W. Nam**[3], **A. C. Wilson**[1], **D. Leibfried**[1], **D. H. Slichter**[1,*]

[1]Time and Frequency Division, National Institute of Standards and Technology, 325 Broadway, Boulder, Colorado 80305, USA

[2]Department of Physics, University of Colorado, Boulder, Colorado 80309, USA

[3]Applied Physics Division, National Institute of Standards and Technology, 325 Broadway, Boulder, Colorado 80305, USA

[4]Department of Physics, University of Oregon, Eugene, Oregon 97403, USA

Abstract

We report high-fidelity state readout of a trapped ion qubit using a trap-integrated photon detector. We determine the hyperfine qubit state of a single ^{9}Be$^+$ ion held in a surface-electrode rf ion trap by counting state-dependent ion fluorescence photons with a superconducting nanowire single-photon detector fabricated into the trap structure. The average readout fidelity is 0.9991(1), with a mean readout duration of 46 μs, and is limited by the polarization impurity of the readout laser beam and by off-resonant optical pumping. Because there are no intervening optical elements between the ion and the detector, we can use the ion fluorescence as a self-calibrated photon source to determine the detector quantum efficiency and its dependence on photon incidence angle and polarization.

Qubit state readout is an essential part of quantum computing and simulation [1,2], including most quantum error correction protocols [3,4]. Trapped ion qubits are typically read out by driving an optical cycling transition with laser light and observing the presence or absence of ion fluorescence [5]. A fraction of the fluorescence photons from the ion are collected, usually with an objective, and imaged onto a photon-counting detector or camera; the number of photons counted over the duration of the readout process indicates the projected state of the qubit. In general, counting just a few percent of the total fluorescence photons from the ion is sufficient to provide readout fidelities in excess of 0.99 [6], and readout fidelities at or approaching 0.9999 have been reported [7–10]. Trapped-ion readout can also be accomplished using state-dependent interactions with a second ion followed by fluorescence readout of that ion, as in quantum logic spectroscopy [11].

*daniel.slichter@nist.gov .
†Present address: Research Laboratory of Electronics, Massachusetts Institute of Technology, Cambridge, Massachusetts 02139, USA.
‡Present address: Department of Physics, University of Washington, Seattle, Washington 98195, USA.

Increasing the number of qubits in trapped-ion quantum processors and simulators can boost computational power, but presents the challenge of reading out the individual states of multiple ions in parallel. One solution is to employ spatially resolved detection, where each ion's fluorescence is ideally imaged onto a separate active detector region. Fluorescence cross talk, where photons from one ion are counted by a detector region dedicated to a different ion, can be tolerated to some degree before the readout fidelity is degraded [8,12,13]. Alternatively, multi-ion readout can be achieved without spatially resolved detection through time-domain-multiplexed illumination of individual ions, for example, by separating ions into different locations in the trap and reading them out in series [14]. This increases the duration of readout in proportion to the number of qubits, limiting utility for many-ion systems.

A number of groups use microfabricated surface-electrode traps [15], which can hold many ions and feature complex designs with multiple trapping zones [16–19], asa path toward large-scale trapped-ion quantum computing. The separate trapping zones can be used for different algorithmic tasks, such as memory, readout, or gate operations [6,19,20]. A natural method for simultaneous readout in such traps is to integrate on-chip photon collection features into the readout zones, such as optical fibers [21], high-numerical-aperture (NA) micro-optics [22–24], or high-reflectivity trap surfaces [25,26]. However, these solutions all rely on separate photon detectors or cameras, and some still require external objectives made with bulk optics. Alternatively, spatially resolved detectors fabricated directly into a surface-electrode trap could perform parallel qubit readout without external collection optics or detectors, with readout signals coupled out of the trap chip as electrical pulses [27–29]. Such a readout architecture frees up the space and optical access used by bulk optics objectives and cameras and potentially enables surface-electrode traps to be tiled in the third dimension, especially when combined with integrated photonics for light delivery [30–32]. It also eliminates the need for imaging system alignment and can, in principle, be scaled to ion traps with many trap zones.

In this Letter, we report the first use of a trap-integrated photon detector for high-fidelity state readout of an ion qubit. We use a superconducting nanowire single-photon detector (SNSPD) cofabricated with a surface-electrode ion trap to detect fluorescence photons at 313 nm from a single ^{9}Be$^+$ ion, achieving qubit state readout with fidelity 0.9991(1) in an average of 46 μs using an adaptive Bayesian readout scheme [7,33]. Using the ion as a tunable, self-calibrating source of photons with known flux and polarization, we characterize the detection efficiency of the SNSPD as a function of incidence angle and polarization, finding agreement with theoretically predicted values. We also study the effect of the trapping rf fields on the SNSPD performance and characterize motional heating of an ion confined over the SNSPD.

SNSPDs are a class of photon detectors with high quantum efficiency [34,35], low dark counts [36,37], and picosecond timing jitter [38]. Recent experiments have shown quantum efficiencies in the UV of 75%–85% at operating temperatures up to 4 K, a parameter regime relevant for ion trap applications [29,36]. Ion fluorescence photons collected with traditional high-NA bulk optics have been counted by a fiber-coupled SNSPD in a stand-alone cryostat to perform fast, high-fidelity qubit readout [39]. However, surface-electrode ion traps present

a challenging electromagnetic and thermal environment for integrated SNSPDs: SNSPDs requiring low-noise bias currents of a few microamperes must be placed close to trap electrodes with rf potentials of tens to hundreds of volts oscillating at up to ~100 MHz. Furthermore, the superconducting transition temperature T_c of the SNSPD should be at least ~25% higher than the temperature at the surface of the trap (typically ≳4 K) to achieve the best detection efficiency [36,40,41]. Combining the separate microfabrication processes for SNSPDs and ion traps while maintaining high device yield and good performance is also a challenge [42]. However, previous work has demonstrated successful integration and operation of SNSPDs on a test chip simulating the thermal and electromagnetic environment of an ion trap [29].

The trap used in this Letter, shown in false color in Fig. 1, is a linear rf (Paul) surface-electrode trap with a SNSPD (green) fabricated on the trap substrate. The rf electrodes (pink) provide confinement transverse to the trap axis [shown as a double-headed black arrow in Fig. 1(b)], while the surrounding segmented electrodes (gray) confine the ion at adjustable positions along the rf null line, from directly over the SNSPD (zone D) to 264 μm away from the SNSPD center (zone A). The ion is held ≈39 μm above the top surface plane of the trap electrodes, dropping by design to a smaller distance of ≈29 μm above this plane when centered over the SNSPD, which is recessed another 6 μm below this plane. The SNSPD consists of a meandered nanowire of 110 nm width on a 170 nm pitch, covering a total active area of 22×20 μm. When the ion is in zone D, this gives an effective NA of 0.32 for the SNSPD; accounting for the dipole emission pattern of the ion fluorescence with the quantization axis as shown in Fig. 1(b), 2.0(1)% of the emitted photons will strike the SNSPD active region [42]. An integrated current-carrying electrode running along the length of the trap between the rf electrodes generates microwave-frequency magnetic fields for qubit control. The trap electrodes are made of electroplated Au on an intrinsic Si substrate, while the SNSPD is made of amorphous $Mo_{0.75}Si_{0.25}$ and has a superconducting transition temperature of 5.2 K [42]. The trap is installed in an ultrahigh-vacuum low-vibration closed-cycle cryostat operated at a temperature of ≈3.5 K [56].

We trap a single $^9Be^+$ ion with typical motional frequencies of ~2 MHz in the axial direction and 5–10 MHz in the radial directions (normal to the trap axis). The potential on the trap rf electrodes has a peak amplitude of 8.8 V at a frequency of 67.03 MHz. A magnetic field of 0.56 mT, in the plane of the trap electrodes and oriented at 45° relative to the trap axis [see Fig. 1(b)], lifts the degeneracy between hyperfine sublevels and defines the quantization axis. This field had no discernible effect on SNSPD performance, consistent with other studies at higher fields [57–59]. We use the $|F = 2, m_F = -2\rangle \equiv |\downarrow\rangle$ and $|F = 1, m_F = -1\rangle \equiv |\uparrow\rangle$ and $|F = 1, m_F = -1\rangle \equiv |\uparrow\rangle$ states within the $2\ ^2S_{1/2}$ hyperfine manifold as our qubit, which has a transition frequency of $\omega_0/2\pi \approx 1.260 \text{GHz}$. We prepare $|\downarrow\rangle$ by optical pumping on the $2\ ^2S_{1/2} \leftrightarrow 2\ ^2P_{3/2}$ transitions at 313 nm with σ^- polarized light. The qubit is read out by detecting fluorescence from the laser-driven $|\downarrow\rangle \leftrightarrow |2^2P_{3/2}, F = 3, m_F = -3\rangle$ cycling transition [42]. Before detection, microwave current pulses on the trap-integrated microwave electrode are used to transfer ("shelve" [5]) population from $|\uparrow\rangle$ to the $|\text{aux}\rangle \equiv |2^2S_{1/2}, F = 1, m_F = 1\rangle$ state for improved

readout fidelity. A pair of counterpropagating laser beams detuned 80 GHz blue of the $2\ ^2S_{1/2} \leftrightarrow 2\ ^2P_{1/2}$ transition at 313 nm are used to drive stimulated Raman transitions on the first-order secular motional sidebands, enabling sideband cooling and motional heating rate measurements [60].

One terminal of the SNSPD is grounded close to the trap chip, while the other is connected via a 50 Ω coaxial cable to room temperature bias and readout electronics [42]. The SNSPD bias current is applied only during readout and is off at other times. The output signal is amplified and filtered to remove parasitic pickup of the trap rf drive before being digitized by a high-speed Schmitt-trigger comparator. The digital pulses are counted and time stamped with 1 ns resolution.

The performance of the SNSPD at 3.45 K was evaluated with the trap rf both off and on. Because an ion cannot be held without trap rf, these measurements were carried out using a simulated ion fluorescence signal generated by laser beam scatter. The beam position and intensity were chosen to give SNSPD count rates similar to those from a single ion in the trap. Figure 2 plots the bright counts (laser on) and dark counts (laser off) during a 200 μs detection window as a function of the applied SNSPD bias current I_b, both with and without trap rf. The I_b at which the critical current density of the superconducting nanowire is exceeded, known as the switching current, is ≈8.9 μA. The trap rf decreases the maximum dc bias current I_m that can be applied without driving the SNSPD to the normal (nonsuperconducting) state. We attribute this reduction to induced rf currents modulating the bias current of the SNSPD [29,42]; a two-parameter fit to a theoretical model for induced rf currents, shown as the blue line, agrees quantitatively with experimental data [42]. Despite the reduction in I_m, the maximum bright counts with the trap rf on are only 17% lower than the maximum bright counts with the rf off. The mean dark counts per detection, both with and without rf, remain below 10^{-2} for I_b at least ~1 μA below the rf-dependent I_m. We emphasize that the dark counts in Fig. 2 are measured in the absence of laser light and are due to residual stray room light or intrinsic detector dark counts [61]. In the experiments described below, the dark count rate is dominated by stray laser light. Qubit control pulses on the microwave electrode with peak power of ~100 mW drive the SNSPD to the normal state even in the absence of bias current, but the SNSPD recovers within a few microseconds of turning off the microwave pulses.

Ion loading occurs in trap zone A, 264 μm from the SNSPD center, and the trapped ion is transported to the detector (zone D) using time-varying potentials on the segmented outer electrodes. When the ion is held above the SNSPD, the detector count rates from ion fluorescence can be combined with knowledge of the excited state lifetime $1/\Gamma = 8.850(2)$ ns [62] of the ion and the ion-detector geometry (including the ion dipole radiation pattern) to provide an absolute calibration of the system detection efficiency (SDE) of the SNSPD. The SDE is defined as the fraction of photons incident on the SNSPD that register as counts in the readout electronics. We vary the intensity of the readout laser beam and fit the corresponding count rates to determine the count rate when the atomic fluorescence transition is driven with a saturation parameter $s \gg 1$ [63]. The background count rate, arising from stray laser scatter not due to the ion, can be subtracted by preparing

the ion in a nonfluorescing state and measuring the count rate. Using this technique, we extract a SDE of 48(2)% with the trap rf on and $I_b = 4\mu$A; accounting for the effects of rf and $I_b < I_m$, this would correspond to a maximum SDE of 65 (5)% without rf [42]. This number is slightly lower than the theoretical design SDE of 72%, potentially due to nanowire oxidation [42].

To characterize the fidelity of the qubit state readout, we prepare the ion in either the fluorescing "bright" $|\downarrow\rangle$ state or the shelved "dark" $|$aux$\rangle$ state and apply the readout laser beam for 500 μs. We record the time stamps of all photons counted during this period, which enables us to vary the readout duration in postprocessing. We use heralding to improve the state preparation fidelity. We define the first 50 μs of the data as the heralding period and retain for further analysis only those trials with zero photon counts in this period as prepared in the dark state and those trials with eight or more photon counts as prepared in the bright state. This method reduces the contribution of state preparation error to the total measurement error. We then analyze the readout fidelity for these trials, using only photon count data from after the heralding period, whose end defines the start of the readout period. Figure 3(a) shows histograms of measured photon counts for both states using a readout duration of 125 μs after the heralding period, with a dotted line showing the threshold number of counts for optimal discrimination of bright and dark states [42]. The fidelity is limited by non-Poissonian tails that cross this threshold, arising from off-resonant pumping of $|$aux$\rangle$ into $|\downarrow\rangle$ and from imperfections in the $\left|\downarrow\right\rangle \leftrightarrow |2^2P_{3/2}, F = 3, m_F = -3\rangle$ cycling transition due to polarization impurity and trap-rf-induced state mixing [42]. The minimum readout error with the thresholding method is $1.2(1) \times 10^{-3}$ at a readout duration of 125 μs. We also analyze the measured state using a variant of the adaptive Bayesian method from Ref. [7]; details are given in the Supplemental Material [42]. As shown in Fig. 3(b), the mean readout duration to reach a given error level is shorter than for the threshold method, and the minimum readout error of $9(1) \times 10^{-4}$, achieved with an average readout duration of 46 μs, is smaller than can be achieved with thresholding. The corresponding maximum readout fidelities are 0.9988(1) and 0.9991(1) for the thresholding and Bayesian methods, respectively.

The motional heating rate of the axial mode was measured in trap zone B, away from the SNSPD, to be 63(6) quanta/s at a frequency of $\omega/2\pi = 2$ MHz, scaling with frequency as $\omega^{-1.7(7)}$. When centered directly over the SNSPD in zone D, the axial mode heating rate was measured to be 113(14) quanta/s at $\omega/2\pi = 5.3$ MHz. Assuming heating rate distance scaling of d^{-4} [64,65] and the measured frequency scaling from zone B, the scaled electric field noise over the SNSPD is estimated to be roughly 6 times higher than that over the gold electrodes, but is still on par with state-of-the-art values reported in cryogenic ion traps [65]. It is unclear whether this increase is due to noise from the wideband SNSPD bias line, to materials properties of the SNSPD, or to some other mechanism.

When the SNSPD outputs a pulse, some portion of the nanowire will stay at ground potential, while the remainder will track the output voltage. This causes a brief impulsive electric field "kick" to the ion, exciting its motion. During readout, this effect can be neglected, as the ion temperature is determined primarily by the scattering of the resonant

readout laser beam from the ion. However, during operations such as stimulated Raman transitions when the ion does not spontaneously emit many photons, SNSPD pulses from stray laser light can become the dominant source of heating. Even when the bias current is off, the SNSPD will occasionally pulse in response to photons when the trap rf is on, as seen in Fig. 2. We measure the resulting heating rate on the 5.3 MHz axial mode in zone D to be 0.009(5) quanta per SNSPD count. This effect limited our ability to perform Raman sideband cooling of an ion held over the SNSPD, due to stray light from the Raman laser beams. In a large-scale processor, operations with high-power Raman beams could be carried out in other trap zones, with the ion(s) transported to the readout zone(s) afterward. The addition of optically transparent SNSPD shielding electrodes may permit operations with high-power Raman beams to be performed in trap zones with integrated SNSPDs, while also reducing induced rf currents in the SNSPDs.

Cross talk from ions in neighboring readout zones will impact the fidelity of parallel readout with trap-integrated SNSPDs. We characterized the cross talk strength by measuring the SNSPD count rate as a function of the ion position along the trap axis. In Fig. 4, we plot the background-subtracted SNSPD count rate when the ion transition is driven with $s \gg 1$, normalized to the highest measured value, as a function of ion distance from the SNSPD center (zone D) along the trap axis [42]. The red curve shows the numerically calculated value assuming constant detector SDE, while the green curve uses a polarization- and incidence-angle-dependent SDE derived from finite element analysis of the SNSPD [42]. The improved agreement between the data and the angle-dependent SDE (versus constant SDE) provides, to the best of our knowledge, the first experimental measurement of the dependence of SNSPD SDE on photon incidence angle. Both theory curves are normalized to the leftmost experimental data point; this overall scaling accounts for experimental reductions in the SDE due to bias currents below I_m and rf pickup [42]. The angle dependence of the SDE would help reduce cross talk errors for parallel qubit readout below the level predicted simply from the solid angle and dipole emission pattern.

Our results provide a path for scalable qubit readout in ion traps. By combining multipixel SNSPD readout [66,67] with trap-integrated photonic waveguides for laser light delivery [30–32], it would be possible to create an ion trap without any free-space optical elements, potentially bringing substantial stability and performance improvements. Such traps could be used not only for large-scale quantum computing, but also for field-deployable quantum sensors, quantum network nodes, or multi-ion optical clocks. Finally, this Letter demonstrates the usefulness of individual trapped ions as well-characterized, tunable, high-precision photon sources for absolute calibration of single-photon detectors.

Acknowledgments

References

[1]. DiVincenzo DP, The physical implementation of quantum computation, Fortschr. Phys 48, 771 (2000).

[2]. Nielsen MA and Chuang IL, Quantum Computation and Quantum Information (Cambridge University Press, Cambridge, England, 2000).

[3]. Preskill J, Fault-tolerant quantum computation, in Introduction to Quantum Computation and Information, edited by Lo H-K, Spiller T, and Popescu S. (World Scientific, Singapore, 1998), pp. 213–269.

[4]. Knill E, Quantum computing with realistically noisy devices, Nature (London) 434, 39 (2005). [PubMed: 15744292]

[5]. Dehmelt HG, Monoion oscillator as potential ultimate laser frequency standard, IEEE Trans. Instrum. Meas 31, 83 (1982).

[6]. Wineland DJ, Monroe C, Itano WM, Leibfried D, King BE, and Meekhof DM, Experimental issues in coherent quantum-state manipulation of trapped atomic ions, J. Res. Natl. Inst. Stand. Technol 103, 259 (1998). [PubMed: 28009379]

[7]. Myerson AH, Szwer DJ, Webster SC, Allcock DTC, Curtis MJ, Imreh G, Sherman JA, Stacey DN, Steane AM, and Lucas DM, High-Fidelity Readout of Trapped-Ion Qubits, Phys. Rev. Lett 100, 200502 (2008).

[8]. Burrell AH, Szwer DJ, Webster SC, and Lucas DM, Scalable simultaneous multiqubit readout with 99.99% single-shot fidelity, Phys. Rev. A 81, 040302(R) (2010).

[9]. Christensen JE, Hucul D, Campbell WC, and Hudson ER, High-fidelity manipulation of a qubit enabled by a manufactured nucleus, npj Quantum Inf. 6, 35 (2020).

[10]. Zhukas LA, Svihra P, Nomerotski A, and Blinov BB, High-fidelity simultaneous detection of trapped ion qubit register, arXiv:2006.12801.

[11]. Schmidt PO, Rosenband T, Langer C, Itano WM, Bergquist JC, and Wineland DJ, Spectroscopy using quantum logic, Science 309, 749 (2005). [PubMed: 16051790]

[12]. Schindler P, Nigg D, Monz T, Barreiro JT, Martinez E, Wang SX, Quint S, Brandl MF, Nebendahl V, Roos CF, Chwalla M, Hennrich M, and Blatt R, A quantum information processor with trapped ions, New J. Phys 15, 123012 (2013).

[13]. Debnath S, Linke NM, Figgatt C, Landsman KA, Wright K, and Monroe C, Demonstration of a small programmable quantum computer with atomic qubits, Nature (London) 536, 63 (2016). [PubMed: 27488798]

[14]. Wan Y, Kienzler D, Erickson SD, Mayer KH, Tan TR, Wu JJ, Vasconcelos HM, Glancy S, Knill E, Wineland DJ, Wilson AC, and Leibfried D, Quantum gate teleportation between separated qubits in a trapped-ion processor, Science 364, 875 (2019). [PubMed: 31147517]

[15]. Seidelin S, Chiaverini J, Reichle R, Bollinger JJ, Leibfried D, Britton J, Wesenberg JH, B Blakestad R, Epstein RJ, Hume DB, Itano W, Jost JD, Langer C, Ozeri R, Shiga N, and Wineland DJ, Microfabricated Surface-Electrode Ion Trap for Scalable Quantum Information Processing, Phys. Rev. Lett 96, 253003 (2006).

[16]. Amini JM, Uys H, Wesenberg JH, Seidelin S, Britton J, Bollinger JJ, Leibfried D, Ospelkaus C, VanDevender AP, and Wineland DJ, Toward scalable ion traps for quantum information processing, New J. Phys 12, 033031 (2010).

[17]. Guise ND, Fallek SD, Stevens KE, Brown KR, Volin C, Harter AW, Amini JM, Higashi RE, Lu ST, Chanhvongsak HM, Nguyen TA, Marcus MS, Ohnstein TR, and Youngner DW, Ball-grid array architecture for microfabricated ion traps, J. Appl. Phys 117, 174901 (2015).

[18]. Maunz PLW, High optical access trap 2.0., Sandia National Laboratories (SNL) Report No SAND2016–0796R, 2016.

[19]. Pino JM, Dreiling JM, Figgatt C, Gaebler JP, Moses SA, Allman MS, Baldwin CH, Foss-Feig M, Hayes D, Mayer K, Ryan-Anderson C, and Neyenhuis B, Demonstration of the QCCD trapped-ion quantum computer architecture, arXiv:2003.01293.

[20]. Kielpinski D, Monroe C, and Wineland DJ, Architecture for a large-scale ion-trap quantum computer, Nature (London) 417, 709 (2002). [PubMed: 12066177]

[21]. VanDevender AP, Colombe Y, Amini J, Leibfried D, and Wineland DJ, Efficient Fiber Optic Detection of Trapped Ion Fluorescence, Phys. Rev. Lett 105, 023001 (2010).

[22]. Merrill JT, Volin C, Landgren D, Amini JM, Wright K, Doret SC, Pai C-S, Hayden H, Killian T, Faircloth D, Brown KR, Harter AW, and Slusher RE, Demonstration of integrated microscale optics in surface-electrode ion traps, New J. Phys 13, 103005 (2011).

[23]. Clark CR, Chou C-W, Ellis AR, Hunker J, Kemme SA, Maunz P, Tabakov B, Tigges C, and Stick DL, Characterization of Fluorescence Collection Optics Integrated with a Microfabricated Surface Electrode Ion Trap, Phys. Rev. Applied 1, 024004 (2014).

[24]. Ghadimi M, Blms V, Norton BG, Fisher PM, Connell SC, Amini JM, Volin C, Hayden H, Pai C-S, Kielpinski D, Lobino M, and Streed EW, Scalable ion-photon quantum interface based on integrated diffractive mirrors, npj Quantum Inf. 3, 4 (2017).

[25]. Herskind PF, Wang SX, Shi M, Ge Y, Cetina M, and Chuang IL, Microfabricated surface ion trap on a high-finesse optical mirror, Opt. Lett 36, 3045 (2011). [PubMed: 21847154]

[26]. Van Rynbach A, Maunz P, and Kim J, An integrated mirror and surface ion trap with a tunable trap location, Appl. Phys. Lett 109, 221108 (2016).

[27]. Leibfried D, Wineland DJ, Blakestad RB, Bollinger JJ, Britton J, Chiaverini J, Epstein RJ, Itano WM, Jost JD, Knill E, Langer C, Ozeri R, Reichle R, Seidelin S, Shiga N, and Wesenberg JH, Towards scaling up trapped ion quantum information processing, Hyperfine Interact. 174, 1 (2007).

[28]. Eltony AM, Wang SX, Akselrod GM, Herskind PF, and Chuang IL, Transparent ion trap with integrated photodetector, Appl. Phys. Lett 102, 054106 (2013).

[29]. Slichter DH, Verma VB, Leibfried D, Mirin RP, Nam SW, and Wineland DJ, UV-sensitive superconducting nanowire single photon detectors for integration in an ion trap, Opt. Express 25, 8705 (2017). [PubMed: 28437948]

[30]. Mehta KK, Bruzewicz CD, McConnell R, Ram RJ, Sage JM, and Chiaverini J, Integrated optical addressing of an ion qubit, Nat. Nanotechnol 11, 1066 (2016). [PubMed: 27501316]

[31]. Niffenegger RJ, Stuart J, Sorace-Agaskar C, Kharas D, Bramhavar S, Bruzewicz CD, Loh W, Maxson RT, McConnell R, Reens D, West GN, Sage JM, and Chiaverini J, Integrated multi-wavelength control of an ion qubit, Nature (London) 586, 538 (2020). [PubMed: 33087912]

[32]. Mehta KK, Zhang C, Malinowski M, Nguyen T-L, Stadler M, and Home JP, Integrated optical multi-ion quantum logic, Nature (London) 586, 533 (2020). [PubMed: 33087915]

[33]. Hume DB, Rosenband T, and Wineland DJ, High-Fidelity Adaptive Qubit Detection through Repetitive Quantum Nondemolition Measurements, Phys. Rev. Lett 99, 120502 (2007).

[34]. Marsili F, Verma VB, Stern JA, Harrington S, Lita AE, Gerrits T, Vayshenker I, Baek B, Shaw MD, Mirin RP, and Nam SW, Detecting single infrared photons with 93% system efficiency, Nat. Photonics 7, 210 (2013).

[35]. Reddy DV, Lita AE, Nam SW, Mirin RP, and Verma VB, Achieving 98% system efficiency at 1550 nm in superconducting nanowire single photon detectors, in The Rochester Conferences on Coherence and Quantum Optics (OSA, Washington, DC, 2019), p. W2B.2, 10.1364/CQO.2019.W2B.2.

[36]. Wollman EE, Verma VB, Beyer AD, Briggs RM, Korzh B, Allmaras JP, Marsili F, Lita AE, Mirin RP, Nam SW, and Shaw MD, UV superconducting nanowire single-photon detectors with high efficiency, low noise, and 4 K operating temperature, Opt. Express 25, 26792 (2017). [PubMed: 29092164]

[37]. Hochberg Y, Charaev I, Nam S-W, Verma V, Colangelo M, and Berggren KK, Detecting Sub-GeV Dark Matter with Superconducting Nanowires, Phys. Rev. Lett 123, 151802 (2019).

[38]. Korzh B. et al. , Demonstration of sub-3 ps temporal resolution with a superconducting nanowire single-photon detector, Nat. Photonics 14, 250 (2020).

[39]. Crain S, Cahall C, Vrijsen G, Wollman EE, Shaw MD, Verma VB, Nam SW, and Kim J, High-speed low-crosstalk detection of a 171Yb+ qubit using superconducting nanowire single photon detectors, Commun. Phys 2, 97 (2019).

[40]. Verma VB, Korzh B, Bussières F, Horansky RD, Lita AE, Marsili F, Shaw MD, Zbinden H, Mirin RP, and Nam SW, High-efficiency WSi superconducting nanowire single-photon detectors operating at 2.5 K, Appl. Phys. Lett 105, 122601 (2014).

[41]. Engel A, Inderbitzin K, Schilling A, Lusche R, Semenov A, Hubers H-W, Henrich D, Hofherr M, Il'in K, and Siegel M, Temperature-dependence of detection efficiency in NbN and TaN SNSPD, IEEE Trans. Appl. Supercond 23, 2300505 (2013).

[42]. See Supplemental Material at http://link.aps.org/supplemental/10.1103/PhysRevLett.126.010501 for additional details of the experimental apparatus, theoretical modeling, and data analysis, which includes Refs. [43–55].

[43]. Annunziata AJ, Quaranta O, Santavicca DF, Casaburi A, Frunzio L, Ejrnaes M, Rooks MJ, Cristiano R, Pagano S, Frydman A, and Prober DE, Reset dynamics and latching in niobium superconducting nanowire single-photon detectors, J. Appl. Phys 108, 084507 (2010).

[44]. Kerman AJ, Rosenberg D, Molnar RJ, and Dauler EA, Readout of superconducting nanowire single-photon detectors at high count rates, J. Appl. Phys 113, 144511 (2013).

[45]. Moharam MG, Gaylord TK, Grann EB, and Pommet DA, Formulation for stable and efficient implementation of the rigorous coupled-wave analysis of binary gratings, J. Opt. Soc. Am. A 12, 1068 (1995).

[46]. Wilson AC, Ospelkaus C, VanDevender AP, Mlynek JA, Brown KR, Leibfried D, and Wineland DJ, A 750-mW, continuous-wave, solid-state laser source at 313 nm for cooling and manipulating trapped $9Be^+$ ions, Appl. Phys. B 105, 741 (2011).

[47]. Burd SC, Penttinen JP, Hou PY, Knaack HM, Ranta S, Mäki M, Kantola E, Guina M, Slichter DH, Leibfried D, and Wilson AC, VECSEL systems for quantum information processing with trapped beryllium ions, arXiv:2003.09060.

[48]. Brandl MF, Schindler P, Monz T, and Blatt R, Cryogenic resonator design for trapped ion experiments in Paul traps, Appl. Phys. B 122, 157 (2016).

[49]. Bourdeauducq S, Whitequark R. Jördens, Sionneau Y, Enjoy-digital C. Ballance T. Harty D. Slichter, Mntng D. Nadlinger R. Srinivas J. Britton Z. Smith K. Stevens F. Held, and Leibrandt D, m-labs/artiq: 3.6, 10.5281/zenodo.1205217 (2018).

[50]. Langer CE, High fidelity quantum information processing with trapped ions, Ph.D. Thesis, University of Colorado, 2006.

[51]. Engel A, Renema JJ, Il'in K, and Semenov A, Detection mechanism of superconducting nanowire single-photon detectors, Supercond. Sci. Technol 28, 114003 (2015).

[52]. Baek B, Lita AE, Verma V, and Nam SW, Superconducting a-W_xSi_{1-x} nanowire single-photon detector with saturated internal quantum efficiency from visible to 1850 nm, Appl. Phys. Lett 98, 251105 (2011).

[53]. Verma VB, Korzh B, Bussières F, Horansky RD, Dyer SD, Lita AE, Vayshenker I, Marsili F, Shaw MD, Zbinden H, Mirin RP, and Nam SW, High-efficiency superconducting nanowire single-photon detectors fabricated from MoSi thin-films, Opt. Express 23, 33792 (2015). [PubMed: 26832040]

[54]. Caloz M, Korzh B, Timoney N, Weiss M, Gariglio S, Warburton RJ, Schönenberger C, Renema J, Zbinden H, and Bussières F, Optically probing the detection mechanism in a molybdenum silicide superconducting nanowire single-photon detector, Appl. Phys. Lett 110, 083106 (2017).

[55]. Jackson JD, Classical Electrodynamics, 3rd ed. (John Wiley, New York, 1999).

[56]. Todaro SL, Improved state detection and transport of trapped ion qubits for scalable quantum computing, Ph.D. Thesis, University of Colorado at Boulder, 2020.

[57]. Korneev A, Korneeva Y, Mikhailov M, Semenov A, Pershin Y, Divochiy A, Vachtomin Y, Smirnov K, Devizenko A, Sivakov A, Gol'tsman G, and Vodolazov D, Characterization of MoSi superconducting single-photon detectors in magnetic field, IEEE Trans. Appl. Supercond 25, 2200504 (2014).

[58]. Korneeva YP, Manova NN, Florya IN, Mikhailov MY, Dobrovolskiy OV, Korneev AA, and Vodolazov DY, Different Single-Photon Response of Wide and Narrow Superconducting Mo_xSi_{1-x} Strips, Phys. Rev. Applied 13, 024011 (2020).

[59]. Polakovic T, Armstrong W, Yefremenko V, Pearson J, Hafidi K, Karapetrov G, Meziani Z-E, and Novosad V, Superconducting nanowires as high-rate photon detectors in strong magnetic fields, Nucl. Instrum. Methods Phys. Res., Sect. A 959, 163543 (2020).

NIST Author Manuscript

NIST Author Manuscript

NIST Author Manuscript

[60]. Monroe C, Meekhof DM, King BE, Jefferts SR, Itano WM, Wineland DJ, and Gould P, Resolved-Sideband Raman Cooling of a Bound Atom to the 3D Zero-Point Energy, Phys. Rev. Lett 75, 4011 (1995). [PubMed: 10059792]

[61]. Yamashita T, Miki S, Makise K, Qiu W, Terai H, Fujiwara M, Sasaki M, and Wang Z, Origin of intrinsic dark count in superconducting nanowire single-photon detectors, Appl. Phys. Lett 99, 161105 (2011).

[62]. Safronova UI and Safronova MS, Relativistic many-body calculation of energies, lifetimes, polarizabilities, and hyperpolarizabilities in Li-like Be$^+$, Phys. Rev. A 87, 032502 (2013).

[63]. Budker D, Kimball DF, and DeMille DP, Atomic Physics, 2nd ed. (Oxford University Press, Oxford, 2008).

[64]. Turchette QA, Kielpinski D, King BE, Leibfried D, Meekhof DM, Myatt CJ, Rowe MA, Sackett CA, Wood CS, Itano WM, Monroe C, and Wineland DJ, Heating of trapped ions from the quantum ground state, Phys. Rev. A 61, 063418 (2000).

[65]. Brownnutt M, Kumph M, Rabl P, and Blatt R, Ion-trap measurements of electric-field noise near surfaces, Rev. Mod. Phys 87, 1419 (2015).

[66]. Zhao Q-Y, Zhu D, Calandri N, Dane AE, McCaughan AN, Bellei F, Wang H-Z, Santavicca DF, and Berggren KK, Single-photon imager based on a superconducting nanowire delay line, Nat. Photonics 11, 247 (2017).

[67]. Wollman EE, Verma VB, Lita AE, Farr WH, Shaw MD, Mirin RP, and Woo Nam S, Kilopixel array of superconducting nanowire single-photon detectors, Opt. Express 27, 35279 (2019). [PubMed: 31878700]
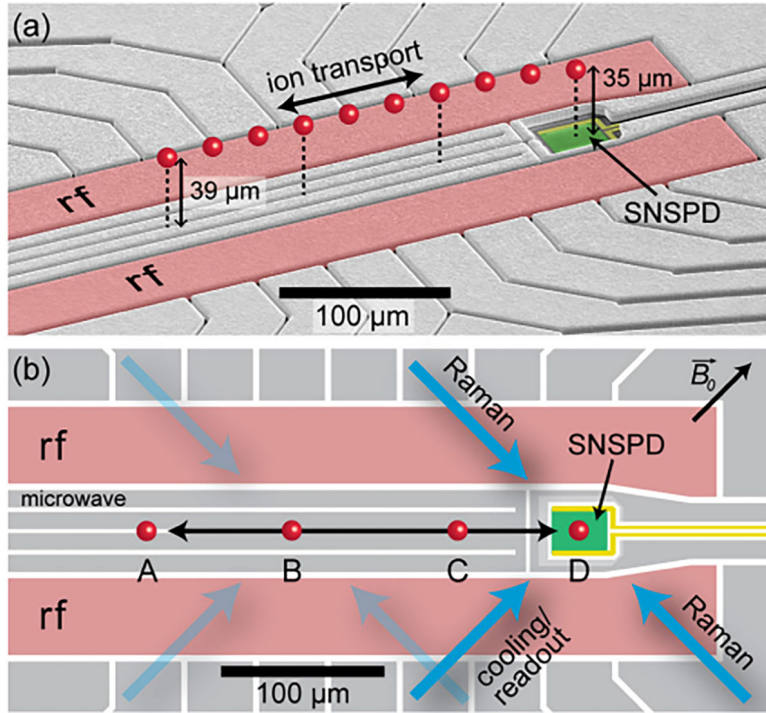
FIG. 1.

Trap configuration. (a) False-color scanning electron micrograph of the ion trap showing the rf electrodes (pink), SNSPD (green), and SNSPD bias leads (yellow). A trapped ion (red sphere, shown in multiple positions along the rf null line) can be transported along the trap axis by applying appropriate time-varying potentials to the outer segmented electrodes (gray). (b) Top view scale diagram showing four labeled trapping zones $A - D$ along the trap axis (double-headed black arrow), as well as the geometry of the laser beams (blue solid arrows, here shown directed at zone D) and quantization magnetic field $\vec{B}_0$, which all lie in the plane of the trap at 45° angles to the trap axis. The laser beams can be translated horizontally to follow the ion as it is transported between zones, as indicated by the faint laser beam arrows directed at zone B.
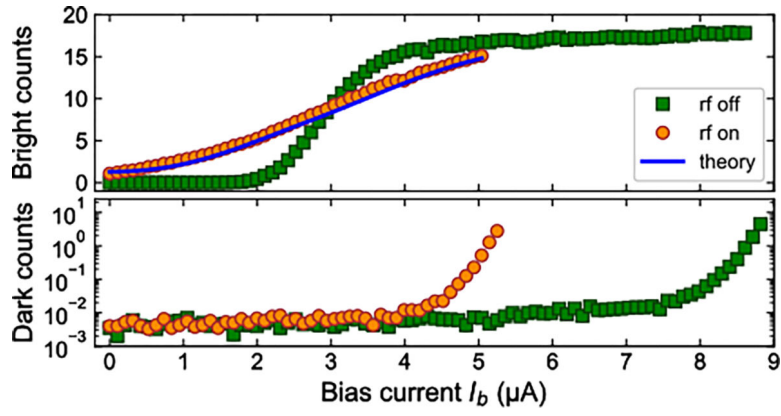
FIG. 2.

Impact of trap rf on SNSPD performance. We plot bright (top) and dark (bottom, log scale) counts in a 200 μs detection window versus SNSPD bias current, with trap rf either off (green squares) or on (orange circles), using laser scatter to simulate ion fluorescence for the bright counts. The blue line is a fit to a theoretical model accounting for induced rf currents in the SNSPD. The bright counts are background-corrected by subtracting the measured dark counts at each bias current. The 68% confidence intervals on the reported values are smaller than the plot symbols.
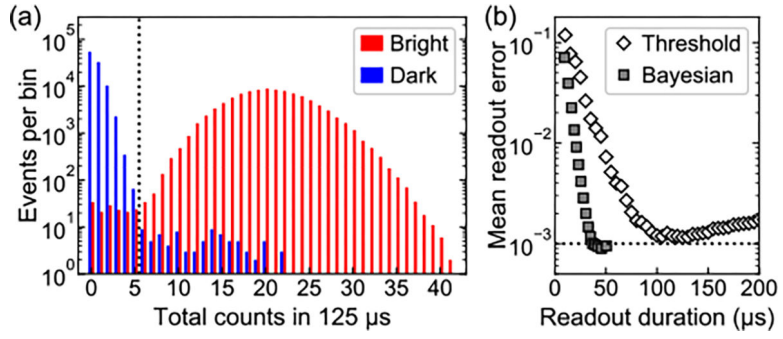
FIG. 3.

Counts and readout error. (a) Count histograms (log scale) for 10^5 trials each of preparing the bright (red) and dark (blue) states, using a 125 μs detection window. The dashed vertical line indicates the optimal threshold for state discrimination. (b) Mean readout error for 2×10^5 trials, half prepared dark and half prepared bright, using either standard thresholding or adaptive Bayesian methods for state determination. For the Bayesian method, the horizontal axis is the mean readout duration before reaching a given state determination confidence level. The dashed horizontal line indicates 10^{-3} mean readout error. Statistical uncertainty in the mean readout error at the 68% confidence level is smaller than the plot symbols.
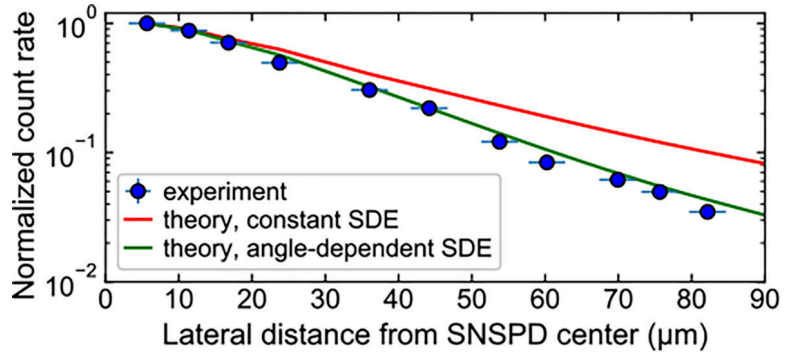
FIG. 4.

Count rate spatial dependence. Moving the ion along the trap axis away from the SNSPD reduces the count rate (blue circles) more strongly than is expected based on detector solid angle and ion dipole radiation pattern alone (red line). Including the calculated angular dependence of SNSPD SDE improves agreement (green line). The 68% confidence intervals on the count rates are smaller than the symbols; those on the theoretical calculations are narrower than the plotted lines.